J Mater Sci (2010) 45:1008–1016
DOI 10.1007/s10853-009-4032-4

Polyacrylamide and poly(acrylamide-co-2-acrylamido-2-methyl-1-propanesulfonic acid)-silica composite nanogels through in situ microemulsion polymerisation

Pallavi Bhardwaj · Vaishali Singh · Uttam Kumar Mandal · Saroj Aggarwal

Received: 18 June 2009 / Accepted: 10 November 2009 / Published online: 21 November 2009

Abstract Nanosize monodisperse composite particles of polyacrylamide (PAM) and poly(acrylamide-co-2-acrylamido-2-methyl-1-propanesulfonic acid)-silica [Poly(AM-co-AMPSA)-SiO_2] were prepared by water-in-oil in situ microemulsion polymerisation without surface treatment of silica. The synthesised composite particles were produced with controllable sizes ranging from 44 to 77 nm in diameter. Presence of silica filler in the nanoreactors facilitates the formation of well-defined discrete particles. The prepared nanocomposites were characterised by dynamic light scattering, transmission electron microscope, Fourier transform infrared spectrophotometer, thermogravimetric analyzer, differential scanning calorimeter, scanning electron microscope and X-ray diffraction. The spectroscopic result shows strong interactions of silica nanoparticles with sulphonic groups of 2-acrylamido-2-methyl-1-propanesulfonic acid (AMPSA). The onset degradation temperature is increased from 227 to 262 °C in copolymer–silica composite as compared to polyacrylamide–silica (PAM–SiO_2) which indicates improved thermal stability. The shifting of glass transition temperature from 194 to 203 °C in copolymeric composite nanogels further confirms the existence of strong interactions of silica filler with poly(acrylamide-co-2-acrylamido-2-methyl-1-propanesulfonic acid) [Poly(AM-co-AMPSA)] chains. Also the chemical composition of polymeric chains and the affinity of polymer chains and silica influenced the morphology of nanogels.

P. Bhardwaj · V. Singh · S. Aggarwal
University School of Basic and Applied Sciences, Guru Gobind Singh Indraprastha University, Kashmere Gate, Delhi 110 403, India

U. K. Mandal (✉)
University School of Chemical Technology, Guru Gobind Singh Indraprastha University, Kashmere Gate, Delhi 110 403, India
e-mail: uttammandal@rediffmail.com

Introduction

Development of colloidal and dispersion science makes a considerable growing field of interest on the applications of organic/inorganic nanosize composite materials. Modification of colloidal suspensions based on the combination of organic and inorganic components, such materials can be designed with a variety of morphologies. The main requirement for the nanosize composite formation involves uniform dispersion and reduced agglomeration of nanoparticles in the organic matrix. A variety of morphological composites (organic/inorganic) have been developed depending on the formation mechanism, surface chemistry and the size of inorganic particles [1, 2].

During the past decade, there has been significant work directed towards the elaboration of nanosize composite particles by embedding inorganic/organic particles in the polymer matrix [3, 4]. The commonly used ultrafine particles for embedment purposes are: three-dimensional nanoparticles (e.g. carbon black, silicon dioxide, titanium dioxide, aluminium oxide), two-dimensional nanofibers (e.g. nanotube, whisker) or one-dimensional disc like nanoparticles (e.g. clay platelets). However, versatility of three-dimensional nanoparticles makes them promising for their wide use in the preparation of polymer nanocomposites. Among three-dimensional nanoparticles, silica nanoparticles have been widely explored. Porous hollow and mesoporous silica nanoparticles find their application in drug release, drug delivery and biosensing application [5, 6]. The current progress in the field is towards multi-fluorescent silica nanoparticles for biological applications

and fluorescent magnetic silica nanoparticles [7, 8] for many biomedical applications such as magnetic resonance imaging, cell separations, etc. The preparation, characterisation, properties and applications of polymer/silica nanosize composites have become a quickly expanding field of research [9–12]. The properties of the nanosize composites strongly depend on their composition, size of the particles, interfacial interaction, etc. [13]. The interfacial interaction between polymer and silica (which depends on the preparative procedures) strongly affects the mechanical, thermal and other properties of the composites. The internal surfaces (interfaces) are critical in determining the properties of nanofilled materials since silica nanoparticles have high surface area-to-volume ratio, particularly when the size decreases below 100 nm. This interfacial area leads to a significant volume fraction of polymer surrounding the particles and has properties different from the bulk polymer. Since this interaction zone is much more extensive for nanocomposites than for microcomposites, it can have significant impact on properties [14].

It is obvious that the important factors that affect the properties of composites are the dispersion and the adhesion at the polymer–filler interface. The surface coating of inorganic nanoparticles with polymer via microemulsion polymerisation is regarded as an effective method to increase dispersing ability and interfacial adhesion simultaneously [15, 16]. Also the microemulsion route through in situ polymerisation reaction carried out in nanostructured media-like micelles allows the synthesis of polymer nanosize composites with controlled architecture and well-defined characteristics [17]. The small particle size and narrow size distribution obtained from inverse microemulsion polymerisation make this method attractive for the synthesis of nanosize composites also [18–20]. To improve the coating efficiency of polymer onto inorganic particles two main strategies are used (i) surface modification of silica particles [21, 22], (ii) incorporation of an auxiliary monomers in the polymerisation process [23, 24].

In our previous work [25] synthesis of nanosize polyacrylamide-silica (PAM–SiO_2) composites by in situ water-in-oil (W/O) microemulsion and their characterisation through various techniques has been reported. There are limited reports on microemulsion polymerisation for the in situ preparation of polymer/silica composites (specially below 100 nm range) [26–28]. Very recently it has been reported that 2-acrylamido-2-methyl-1-propanesulfonic acid (AMPSA) is a good candidate as a clay modifier for the preparation of polymer–clay nanocomposites by in situ free radical polymerisation in emulsion [29]. The use of a low percentage of AMPSA as a speciality monomer seems to play a major role in achieving successful exploitation of silica in preparation of polymer–silica nanosize composites by in situ polymerisation in microemulsion. The purpose of our present study is to investigate the effect of AMPSA incorporation in polymer chain on size, interaction, thermal stability and morphology of nanosize silica composite particles without surface treatment of silica. On the basis of microemulsion stability, we have synthesised Poly(AM-co-AMPSA) nanosize composites by in situ W/O microemulsion process taking 5.5 mol.% of AMPSA in feed. The prepared composites have been characterised by dynamic light scattering (DLS), Fourier transform infrared spectrophotometer (FTIR), thermogravimetry analyzer (TGA), differential scanning calorimeter (DSC), scanning electron microscope (SEM), transmission electron microscope (TEM) and X-ray Diffraction (XRD). The results have also been compared with PAM–SiO_2 composite particles.

Experimental

Materials

Acrylamide (AM), AMPSA, 10 nm silicon dioxide (SiO_2), sodium bis(2-ethylhexyl)sulfosuccinate (AOT) were purchased from Aldrich and used directly without further purification. 2,2-azobisisobutyronitrile (AIBN) purchased from Spectrochem Private Ltd. (India) and extra pure *N*,*N*′-methylenebisacrylamide (NMBA) from SRL (India) were used as an initiator and a crosslinker, respectively. AR grade toluene, received from SRL (India) was distilled prior to use. Double-distilled water drawn from a Millipore purification system was used.

Preparation of composite nanogels

The aqueous phase of microemulsion system was obtained by dissolving desired amount of AM and AMPSA in 12.70 mL of water (Table 1). 0.191 g silica was dispersed in aqueous solution of monomer(s) and it was stirred on a magnetic stirrer at 1000 rpm for 2 h to attain proper dispersion of silica in the solution of monomer(s). The dispersion medium of microemulsion was made by dissolving 23.84 g AOT in 59.64 g toluene and the aqueous solution of monomer(s) containing disperse SiO_2 was added dropwise to the surfactant solution to form a W/O microemulsion. The polymerisation was carried out in 250 mL, two-neck round-bottom flask fitted with a condenser and a nitrogen gas inlet. The solution was stirred on magnetic stirrer at 1000 rpm for 6 h. AIBN and NMBA (each 1 wt% of monomers) were added to initiate the polymerisation and for crosslinking. The microemulsion was then purged with nitrogen gas for 30 min. The polymerisation mixture was then heated in a constant temperature water bath at

Table 1 The composition of W/O microemulsion used for synthesis

Composition (gm)	Samples			
	PAM	PAM–SiO_2	Poly(AM-co-AMPSA)	Poly(AM-co-AMPSA)-SiO_2
Toluene	59.64	59.64	59.64	59.64
AOT	23.84	23.84	23.84	23.84
Water	12.70	12.70	12.70	12.70
AM	3.82	3.82	3.25	3.25
AMPSA	0.00	0.00	0.57	0.57
SiO_2	0.00	0.191	0.00	0.191
AIBN	0.0382	0.0382	0.0382	0.0382
NMBA	0.0382	0.0382	0.0382	0.0382

50 °C for copolymer and copolymer composites while at 62 °C for PAM nanogels and PAM composites till complete conversion. After polymerisation the mixture was cooled to room temperature and methanol was added to precipitate the polymerised product. The precipitates were separated out and washed several times through centrifugation first with methanol to remove residual monomer and then with toluene to remove AOT. The precipitates were then dried in vacuum oven at 50 °C till constant weight was obtained. PAM and copolymer nanogels were also prepared in similar way without silica.

Characterisation

A Malvern Zetasizer Nano Series ZEN 1600 (Malvern Instruments Limited, UK) was used to measure the size of the reverse micelle of microemulsion, nanogels and composites. DLS measurements were performed at 25 °C in a square glass cuvette with round aperture at a fixed angle of 173°. The value of dispersant refractive index and viscosity of toluene were taken 1.491, 0.5500 cP, respectively.

A transmission electron microscope (Morgagni 268D TEM, The Netherlands) with a 70 kV accelerating voltage was used to measure the size of the prepared nanosize composites. The aqueous dispersions of composite particles were sonicated at 25 °C then dried onto carbon-coated 400 mesh copper grids.

The FTIR spectra were collected on SHIMADZU Japan FTIR-8700 Fourier-transform infrared spectrophotometer in the range of 4400–400 cm^{-1}.

The thermogravimetric analysis was performed using a Perkin-Elmer TGA7 thermobalance. The dried samples in a nitrogen atmosphere were analysed in the temperature range of 50–800 °C at scanning rate of 20 °C/min.

DSC Q10, TA Instruments, USA was used to study the glass transition temperature. About 2 mg of the sample was sealed in an aluminium DSC pan and heated from 50 to 350 °C at a heating rate of 10 °C/min under nitrogen purge flow (50 mL/min).

The surface morphology of the dried nanogels and composites were studied by using scanning electron microscope (LEO 435 VP) operated at 15 kV. Coating was carried out under reduced pressure in an inert argon gas atmosphere (Agar Sputter Coater P7340).

X-ray diffraction measurements of powdered nanogels and composites were carried out using an X-ray diffractor unit (Philips PW3040/60 X'pert PRO PANalytical-Netherlands) with Nickel filtered Cu Kα radiation at 1.54. The resultant intensity data was processed using in-built PC-APD diffraction software to monitor the peak position and its intensity. The samples were placed on a glass slide and the measurements were taken continuously from 5° to 80° angles.

Results and discussion

DLS Analysis

The particle size and PDI of pure PAM, PAM–SiO_2, Poly(AM-co-AMPSA) and Poly(AM-co-AMPSA)-SiO_2 as synthesised in microemulsion measured by DLS and in dry state measured by TEM are reported in Table 2. The size distribution of the same has also been shown in Fig. 1. Compared to size of monomer laden micelles (around 10 nm) in microemulsion environment, the size of nanogels/composites dispersed in toluene are found to be larger

Table 2 Size of nanogels as synthesised in microemulsion measured by DLS and in dry state measured by TEM

Samples	PDI	Size measurement by DLS (nm)	Size measurement by TEM (nm)
PAM	0.243	63	55
PAM–SiO_2	0.171	44	40
Poly(AM-co-AMPSA)	0.314	105	90
Poly(AM-co-AMPSA)-SiO_2	0.378	77	60

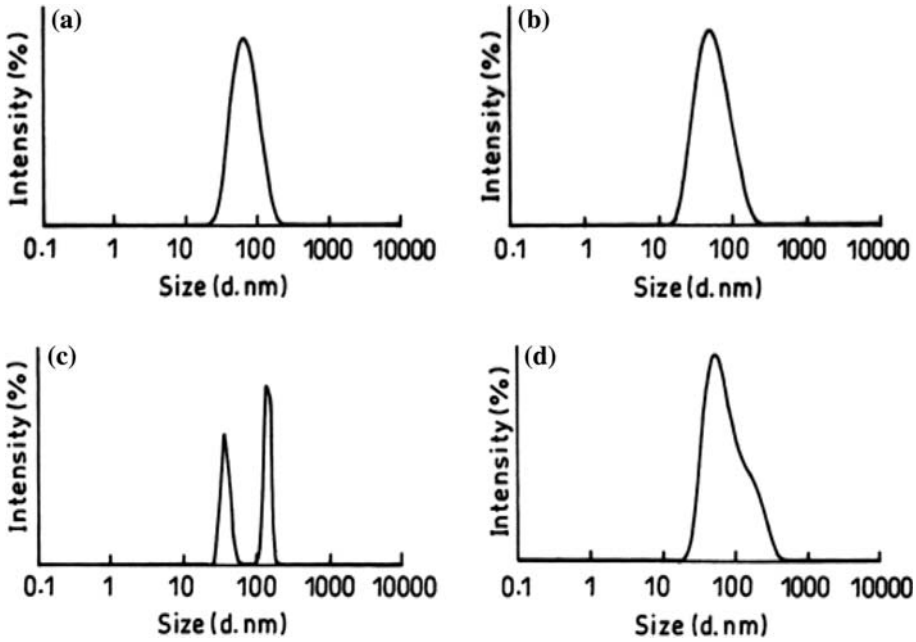

Fig. 1 Size distribution curves of **a** PAM, **b** PAM-SiO_2, **c** Poly(AM-co-AMPSA), **d** Poly(AM-co-AMPSA)-SiO_2

as reported in the literature [30]. The increase in diameter is attributed to micelle collisions occurring during free radical polymerisation producing a nanogel/composite which comprises of multiple reacting monomer micelles. This hypothesis is consistent with mechanistic models reported in the literature for inverse microemulsion polymerisation of monomers that do not partition in the continuous phase [31, 32]. It is also evident that the presence of acidic monomer in Poly(AM-co-AMPSA) nanogels shows higher size of particle than pure PAM particles. This may be due to higher swelling of copolymer in microreactors in toluene continuous phase with limited water droplets as incorporation of AMPSA increases the hydrophilicity of the particles leading to higher solvation. In presence of silica filler in in situ polymerisation state of PAM and copolymer causes reduction in size of corresponding PAM composite and copolymer composite, respectively. Decrease in particle size is attributed to homogenous dispersion of silicon dioxide in surfactant solution in such a manner that SiO_2 was spread to the fullest both in and around the PAM and copolymer [25, 33]. The size of nanogels and their respective nanosize composites obtained from DLS are in good agreement with transmission electron microscopy analysis (Fig. 2i, ii). The little higher size of as-synthesised nanogels measured by DLS than measurement by TEM may be due to apparent swelling in limited aqueous phase present in microreactors.

FTIR analysis

The FTIR spectra of PAM, PAM–SiO_2, Poly(AM-co-AMPSA) and Poly(AM-co-AMPSA)-SiO_2 in absorbance mode are shown in Fig. 3. The bending (or scissoring) motion of saturated –CH_2 group gives a band of medium to strong intensity between 1416 and 1429 cm^{-1}. The N–H stretching of amide group in AM and overlapping O–H stretching of sulfonic acid group in AMPSA is observed in the region 3200–3500 cm^{-1} [34]. C=O stretching of CO in both AM and AMPSA shows strong band in the region 1652–1668 cm^{-1}. The peak in the region of 1616 cm^{-1} corresponds to N–H bending of NH_2 (δ) in PAM and PAM–silica [35]. Secondary amide II band, asymmetric bands of SO_2 and sulfonic acid (–SO_3H) of AMPSA in Poly(AM-co-AMPSA) occurs at 1550, 1194, 1041 cm^{-1}, respectively. The peak in the range 475–481 cm^{-1} in Poly(AM-co-AMPSA)-SiO_2 attributes to Si–O–Si bending vibrations [36]. Hence presence of important groups such as C=O, –$CONH_2$, –CONH, –SO_3H, Si–O and absence of olefinic band in the range 1620–1635 cm^{-1} confirms that product contains Poly(AM-co-AMPSA) along with silica units and excludes the presence of monomer. The main characteristic peaks of FTIR spectra are shown in Table 3.

The Si–O–Si asymmetric band stretching vibration of silica occurs at 1098 cm^{-1} [37, 38]. However, in copolymer–silica the peak at 1098 cm^{-1} is not present but a strong peak at 1041 cm^{-1} is found in the spectrum which may be due to combination of strong hydrogen bonded Si–O with sulphonic group. All silica nanoparticles are coated with copolymer chain and absence of peak at 1098 cm^{-1} may indicate the absence of free silica in the composites. Nitrogen atom being less electronegative than oxygen atom, the electron pair on nitrogen atom in PAM is more labile and participates in conjugation. Due to this conjugation, the C=O absorption frequency is much less in PAM

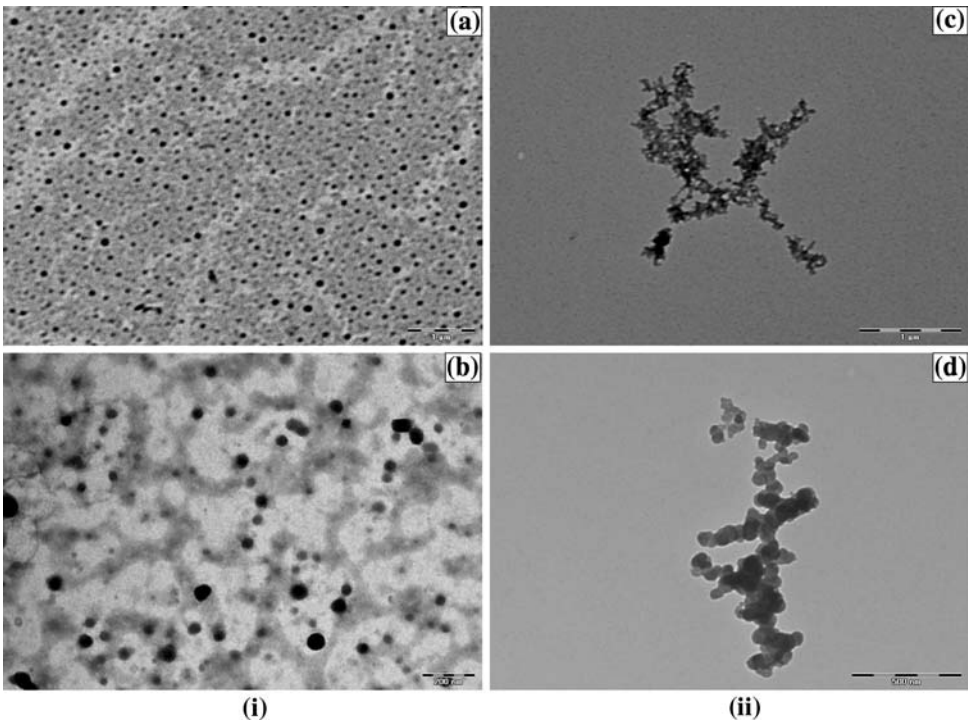

Fig. 2 (i) TEM micrographs of **a** PAM, **b** PAM–SiO_2. (ii) TEM micrographs of **c** Poly(AM-co-AMPSA), **d** Poly(AM-co-AMPSA)-SiO_2

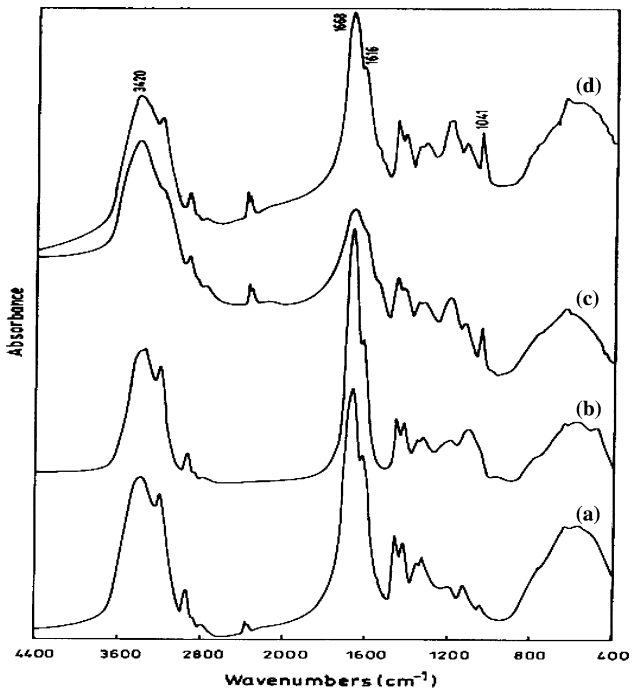

Fig. 3 The FTIR spectra in the range 4400–400 cm^{-1} of (*a*) PAM, (*b*) PAM–SiO_2, (*c*) Poly(AM-co-AMPSA), (*d*) Poly(AM-co-AMPSA)-SiO_2

(1652 cm^{-1}) and copolymer (1655 cm^{-1}). However, C=O absorption frequency in their counterparts PAM–silica and copolymer–silica is at 1662 and 1668 cm^{-1}, respectively, which is attributed to no more labile nature of electron pair on nitrogen on account of hydrogen bonding between the amino groups in the polymer molecules and Si–O linkage and therefore no participation in conjugation [39].

Table 3 Specific FTIR peaks of PAM, Poly(AM-co-AMPSA) and their silica composites

Peak position in cm^{-1}	Assignment
3200–3500	N–H stretching of NH_2 (ν), OH stretching of $–SO_3H$ acid group
1652–1668	C=O stretching of CO in AM, AMPSA
1616	N–H bending of NH_2 (δ) in AM
1550	Secondary amide II band of AMPSA
1416–1429	$–CH_2$ bending
1194	Asymmetric band of SO_2
1041	$–SO_3H$ acid group
1098	Si–O–Si asymmetric stretching
475–481	Si–O–Si bending vibration

The increment in sites for SiO_2 attachment promotes high degree of attachment of filler to the chain. Moreover, in situ incorporation of silica in copolymer sample promotes better dispersion of filler and stronger interaction with the copolymer chains through hydrogen bonding. Also another mechanistic model may be cause for better dispersion of filler particles through adsorption of monomer on filler surface and polymerisation first starts on the filler surface through adsorbed AMPSA monomer and continues thereafter [29].

Table 4 DTG results of PAM, Poly(AM-co-AMPSA) and their silica composites

Samples	Temperature of initiation (T_i) (°C)	I Peak temperature (T_{Imax}) (°C)	II Peak temperature (T_{IImax}) (°C)	III Peak temperature (T_{IIImax}) (°C)
PAM	227	300	401	627
PAM–SiO_2	227	295	400	642
Poly(AM-co-AMPSA)	228	333	412	652
Poly(AM-co-AMPSA)-SiO_2	262	347	424	–

TGA analysis

It is evident that the degradation of PAM-filled is affected by the presence of small dose of AMPSA in copolymer-filled composite. The temperature of onset of degradation is 227 °C for PAM–silica and 262 °C for copolymer–silica, indicates improved thermal stability of the copolymer composites (Table 4). This shows the active contribution of AMPSA towards enhancing the stability of composites. Polymers containing $-SO_3^-$ groups are expected to offer higher stability in solution, on account of their stronger hydrogen bonding [40]. The geminal dimethyl group and the sulfomethyl group combine to sterically hinder the amide functionality and provide thermal stabilities to AMPSA-containing polymers [41–43]. Though thermal stability is not required for any bio-application but these type of composites may find their application in oil recovery. To improve oil recovery, Yang-Chuan et al. [44] prepared nanocomposites of AM–styrene–AMPSA copolymers with monodisperse silica particles.

PAM–silica composites degraded in three main steps at 295 °C (T_{Imax}), 400 °C (T_{IImax}) and 642 °C (T_{IIImax}). However, two distinct peaks at around 347 °C (T_{Imax}) and 424 °C (T_{IImax}) are identified in copolymer–silica composites. These peaks are attributed to possible degradation of sulfonic groups and breakdown of polymer backbone, respectively. The third peak in PAM–silica at 642 °C (attributed to random bond scission of the polymeric main chain) disappears vividly from copolymer–silica. This is attributed to the role of silica nanoparticles which actively form strong interactions with functional groups of copolymer and thus preventing the degradation of the main polymeric chain at that temperature. T_{Imax} and T_{IImax} shifted from 295 to 347 °C and from 400 to 424 °C when silica is incorporated in PAM and copolymer, respectively.

Typical weight loss (TG) curves of PAM, PAM–SiO_2, Poly(AM-co-AMPSA) and Poly(AM-co-AMPSA)-SiO_2 are shown in Fig. 4. Aggour [42] reported that Poly(AM-co-AMPSA) copolymers show thermal degradation in three stages: decomposition of amide groups, degradation of sulfonic groups and breakdown of polymer backbone. However, the TGA curves of nanogels/composites show four stages of weight loss. The first stage weight loss is found to be 5–14% from 47 to 206 °C. This weight loss is due to removal of adsorbed water in the sample [45]. Though first stage weight loss is due to loss of water but there is less moisture content in copolymer–silica. The second stage weight loss is 13–27% from 206 to 378 °C. At this stage irreversible chemical changes may occur due to thermal degradation [46]. The weight loss in this region is attributed to both intra- and intermolecular imidization reactions. The third stage decomposition is 23–47% from 348 to 520 °C. In this region degradation of the polymer main chain occurs. It seems that the polymer chains in the intricated network of composites are protected from thermo-oxidative process. The last stage decomposition is 8–39% from 503 to 800 °C. After this stage the residue content shows ascending trend, i.e. 0, 3.28, 3.98 and 27%, respectively. The presence of inorganic component/filler retards the degradation of copolymer–silica. The copolymer composites therefore show better thermal stability as compared to PAM–silica composites. The marked increase in residue for copolymer–silica is attributed to uniform dispersion through in situ microemulsion polymerisation

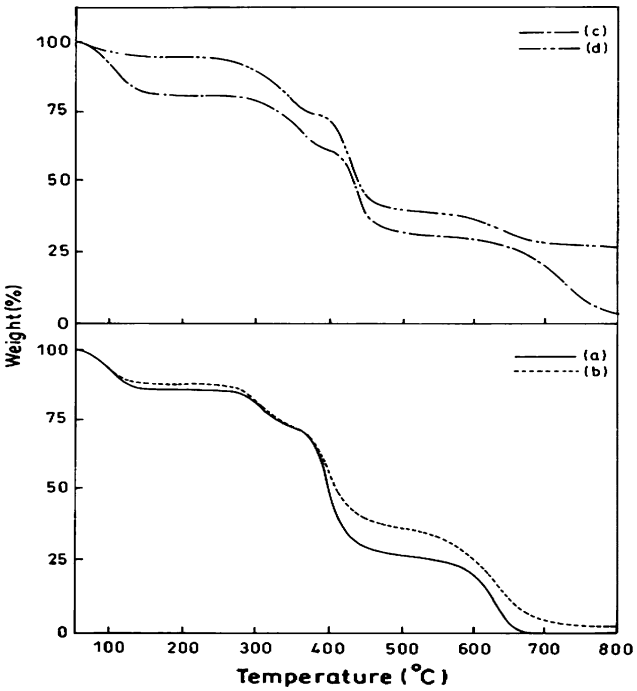

Fig. 4 TGA curves of (*a*) PAM, (*b*) PAM–SiO_2, (*c*) Poly(AM-co-AMPSA), (*d*) Poly(AM-co-AMPSA)-SiO_2

and consequently a high degree of attachment of silica nanoparticles to polymer chain. The high char formation in copolymer–silica composites reduces the production of gases and decreases the exothermicity of the reactions. This advantage offers application of copolymer-inorganic composites to fulfil the demands of high melting blend nanosize composites.

DSC analysis

The DSC thermograms of PAM, PAM–SiO_2, Poly(AM-co-AMPSA) and Poly(AM-co- AMPSA)-SiO_2 are shown in Fig. 5. From these thermograms, the glass transition temperature (T_g), the decomposition temperature (T_{Imax} and T_{IImax}) and the decomposition enthalpy (ΔH_{d1} and ΔH_{d2}) have been calculated. The transition temperature (T_g) and heat flow corresponding to decomposition zones are reported in Table 5. The homopolymer and its filled composite show two endotherm peaks while three peaks are present in the copolymer and its filler based composite. As reported in our previous work [25] the occurrence of peak in the range 59–103 °C is attributed to loss of water. It is also evident that the temperature and area of the first peak have been considerably reduced on account of filler loading in PAM and Poly(AM-co-AMPSA) copolymer nanogels. The second region endotherm peaks are in the range 266–287 °C and attributed to amide group degradation and the cleavage of weak crosslinks [47].

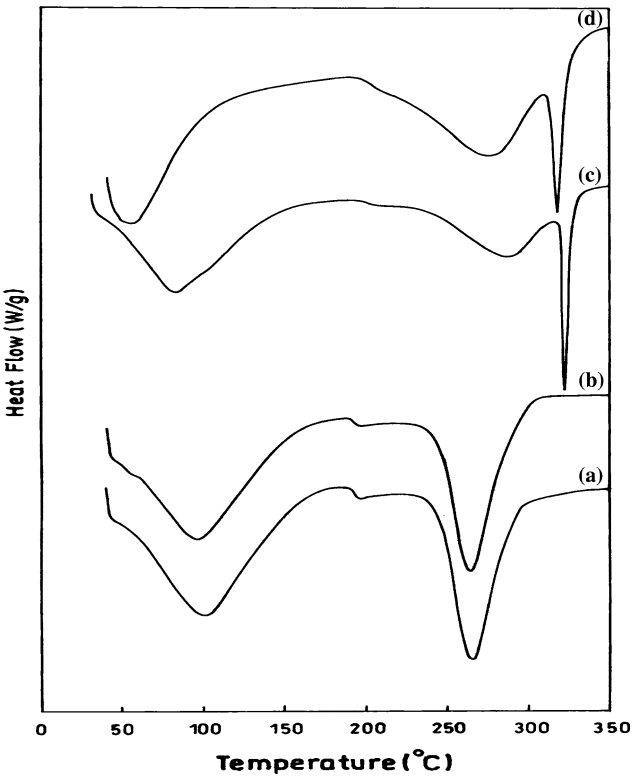

Fig. 5 DSC curves of (*a*) PAM, (*b*) PAM-SiO_2, (*c*) Poly(AM-co-AMPSA), (*d*) Poly(AM-co-AMPSA)-SiO_2

Figure 5 also shows that the onset of degradation (235 °C) for homopolymer-filled composite and reaches at maximum peak 265 °C (T_{Imax}) whereas in copolymer-filled composite, the onset of degradation is at 216 °C and it reaches at 277 °C (T_{Imax}). The degradation peak at 321 °C (T_{IImax}) and 318 °C (T_{IImax}) in copolymer and its composite is attributed to the degradation of sulfonic groups. The T_{IImax} of copolymer-filled has shifted to lower side as the sulfonic group makes H-bonding with the silica filler weakens the linkage of these groups with the polymer chains.

From the figure it is also depicted that the second order transition, i.e. glass transition temperature (T_g) shows increment in the order 191.95, 193.56, 196.63 and 203.18 °C for pure PAM, PAM–SiO_2, Poly(AM-co-AMPSA) and Poly(AM-co-AMPSA)-SiO_2, respectively. Higher T_g (196.63 °C) of copolymer is due to presence of sterically bulky propane sulfonic group which hinders bond rotation and presence of strong H-bonding in copolymer chains. However, there is a dramatic increase in the T_g for filler laden copolymer. This is perhaps due to strong reinforcement of filler polymer chain interaction to a greater extent. The incorporation of nanosize silica powder (10 nm) promotes strong interaction with copolymeric chains and resists changes in the conformation of the polymeric chain at the nano level. Moreover, there is confinement of polymer chains to domains smaller than 15 nm, thus the characteristic longer motions of the glass transition are restricted. This indicates that it possesses very fine-grained, interpenetrating copolymer–silica morphologies [48].

Table 5 Thermal properties obtained by DSC of PAM, Poly(AM-co-AMPSA) and their silica composites

Samples	Initiation temperature (T_i) (°C)	T_g (°C)	I Peak temperature (T_{Imax}) (°C)	ΔH_{d1} (J/g)	II Peak temperature (T_{IImax}) (°C)	ΔH_{d2} (J/g)
PAM	231	191.95	266	229	–	–
PAM–SiO_2	235	193.56	265	273	–	–
Poly(AM-co-AMPSA)	236	196.63	288	135	321	73
Poly(AM-co-AMPSA)-SiO_2	216	203.18	277	173	318	68

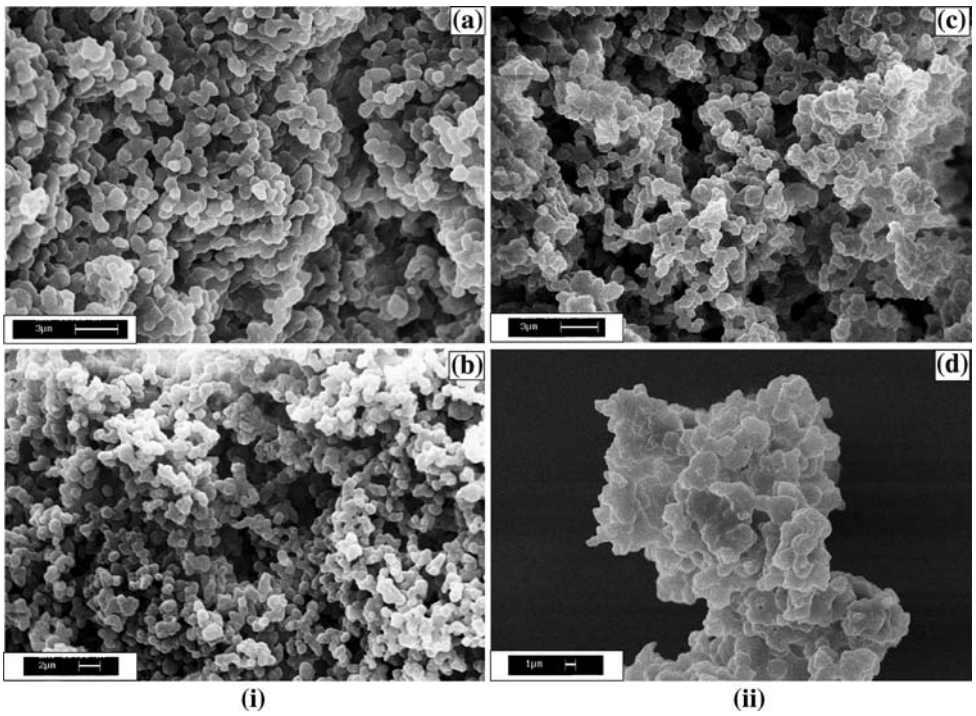

Fig. 6 (i) SEM micrographs of **a** PAM, **b** PAM–SiO_2. (ii) SEM micrographs of **c** Poly(AM-co-AMPSA), **d** Poly(AM-co-AMPSA)-SiO_2

SEM analysis

Figure 6i and ii shows the scanning electron micrographs of PAM and copolymer along with nanosize composites. The micrographs are in the high magnification range which allow us to better understand the morphology and topography. In Fig. 6i (a) pure PAM nanogels have smooth surface with loose structure while Fig. 6i (b) for PAM–SiO_2 composites shows more smaller particle size with isolated form. The morphology of Poly(AM-co-AMPSA) nanogels in Fig. 6ii (c) has changed gradually to elongated cylindrical shape. Further, incorporation of filler in copolymer results in composite with definite elongated geometrical boundaries Fig. 6ii (d).

XRD analysis

The XRD of nanosilica did not display any crystalline peaks, which was consistent with the silica nanoparticles being non crystalline at that scale [49]. It clearly indicates that silica is in the amorphous state. PAM has strong Bragg reflections, the crystalline peaks appear in the 2θ range 22°–43° [50]. PAM has high degree of crystallinity [51] but copolymer formation has shifted crystallinity towards more amorphous side. Poly(AM-co-AMPSA) shows extended amorphous region leading to disruption of ordered chains of pure PAM and further the addition of silica to copolymer increases the amorphous nature of copolymer and restricts the alignment of polymer chains due to strong interaction of silica nanoparticle with polymer chains.

Conclusions

In situ microemulsion process retards the tendency of silica nanoparticles to agglomerate and makes the distribution of the inorganic filler more homogenous, consequently reducing the size of functionalized composite. The presence of AMPSA content shifts the degradation temperature of the nanosize composite to the higher side. Spectroscopic as well as measurement of glass transition temperature indicates very strong interactions between silica filler and copolymer chains containing sulfonic groups. SEM analysis shows discernible change in morphology upon incorporation of AMPSA with filler, i.e. geometrical pattern.

References

1. Yang M, Dan Y (2005) Colloid Polym Sci 284:243
2. Beecroft LL, Ober CK (1997) Chem Mater 9:1302
3. Rigbi Z (1980) Adv Polym Sci 36:21
4. Ettlinger M (1989) Schriftenreihe Pigmente 56:2
5. Li ZZ, Ding HM, Wang JX, Chen JF (2006) J Nanosci Nanotechnol 6:3139
6. Slowing II, Trewyn BG, Giri S, Lin VS-Y (2007) Adv Funct Mater 17:1225
7. Nakamura M, Shono M, Ishimura K (2007) Anal Chem 79:6507
8. Yang J, Lee J, Kang J, Chung CH, Lee K, Suh JS, Yoon HG, Huh YM, Haam S (2008) Nanotechnology 19:1
9. Althues H, Henle J, Kaskel S (2007) Chem Soc Rev 36:1454
10. Sanchez C, Julian B, Belleville P, Popall M (2005) J Mater Chem 15:3559
11. Pomogailo AD (2000) Russ Chem Rev 69:53

12. Radhakrishnan B, Ranjan R, Brittain WJ (2006) Soft Matter 2:386
13. Gao Y, Choudhury NR (2003) In: Nalwa HS (ed) Handbook of organic-inorganic hybrid materials and nanocomposites, vol 1. American Scientific Publishers, Stevenson Ranch, CA, p 271
14. Roy M, Nelson JK, MacCrone RK, Schadler LS, Reed CW, Keefe R, Zenger W (2005) IEEE Trans Dielectr Electr Insul 12:629
15. Pavel FM (2004) J Disper Sci Technol 25:1
16. Yan F, Texter J (2006) Soft Matter 2:109
17. Gianini M, Caseri WR, Suter UW (2001) J Phys Chem B 105:7399
18. Puig LJ, Sanchez-Diaz JC, Villacampa M, Mendizabal E, Puig JE, Aguiar A, Katime I (2001) J Colloid Interface Sci 235:278
19. Fernandez VVA, Tepale N, Sanchez-Diaz JC, Mendizabal E, Puig JE, Soltero JFA (2006) Colloid Polym Sci 284:387
20. Kaneda I, Sogabe A, Nakajima H (2004) J Colloid Interface Sci 275:450
21. Cheng W, Wang Z, Ren C, Chen H, Tang T (2007) Mater Lett 61:3193
22. Xu P, Wang H, Tong R, Du Q, Zhong W (2006) Colloid Polym Sci 284:1435
23. Yang J, Hu D, Fang Y, Bai C, Wang H (2006) Chem Mater 18:4902
24. Ranjan R, Brittain WJ (2007) Macromolecules 40:6217
25. Bhardwaj P, Singh S, Singh V, Aggarwal S, Mandal UK (2008) Int J Polym Mater 57:404
26. Yu J, Yu J, Gao YF, Guo ZX (2001) Chin J Polym Sci 20:71
27. Chow PY, Gan LM (2004) J Nanosci Nanotechnol 4:197
28. Xu P, Wang HT, Tong R, Du QG, Zhong W (2006) Colloid Polym Sci 284:755
29. Greesh N, Hartmann PC, Cloete V, Sanderson RD (2008) J Colloid Interface Sci 319:2
30. Mc Allister K, Sazani P, Adam M, Cho MJ, Rubinstein M, Samulski RJ, Desimone JD (2002) J Am Chem Soc 124:15198
31. Buruaga ASD, Cal JDL, Asua JM (1999) J Polym Sci Part A: Polym Chem 37:2167
32. Buruaga ASD, Capek I, Cal JDL, Asua JM (1998) J Polym Sci Part A: Polym Chem 36:737
33. Voorn DJ, Ming W, van Herk AM (2006) Macromolecules 39:2137
34. Zhang C, Easteal AJ (2007) J Appl Polym Sci 104:1723
35. Lu X, Mi Y (2005) Macromolecules 38:839
36. Wu Z, Lee K, Lin Y, Lan X, Huang L (2003) J Non-Cryst Solid 320:168
37. Jang J, Park H (2002) J Appl Polym Sci 83:1817
38. Elbatal HA, Azooz MA, Khalil EMA, Monem AS, Hamdy YM (2003) Mater Chem Phys 80:599
39. Silverstein RM, Webster FX (1998) Spectrometric identification of organic compounds. Wiley, New York
40. Sabhapondit A, Borthakur A, Haque I (2003) J Appl Polym Sci 87:1869
41. Parker WO Jr, Lezzi A (1993) Polymer 34:4913
42. Aggour YA (1994) Polym Degrad Stab 44:71
43. Aggour YA (1998) Polym Degrad Stab 60:317
44. Yang-Chuan K, Guang-Yao W, Yi W (2008) Eur Polym J 44:2448
45. Vilcu R, Irinei F, Ionescu-Bujor J, Olteanu M, Demetrescu I (1985) J Therm Anal 30:495
46. Van Dyke JD, Kasperski KL (1993) J Polym Sci Part A: Polym Chem 31:1807
47. Zhang C, Easteal AJ (2003) J Appl Polym Sci 89:1322
48. Amalvy JI, Percy MJ, Armes SP (2001) Langmuir 17:4770
49. Petrovic ZS, Javni I, Waddon A, Banhegyi GJ (2000) J Appl Polym Sci 76:133
50. Biswal DR, Singh RP (2004) Carbohydr Polym 57:379
51. Yan F, Zheng C, Zhai X, Zhao D (1998) J Appl Polym Sci 67:747